Δ degrees of freedom in antisymmetrized molecular dynamics and (p,p') reactions in the Δ region

Andreas Engel, Eiji I. Tanaka, Tomoyuki Maruyama,* Akira Ono,† and Hisashi Horiuchi
Department of Physics, Kyoto University, Kyoto 606-01, Japan
(Received 17 May 1995)

Δ degrees of freedom are introduced into antisymmetrized molecular dynamics (AMD). This is done by increasing the number of basic states in the AMD wave function, introducing a Skyrme-type delta-nucleon potential, and including $NN \leftrightarrow N\Delta$ reactions in the collision description. As a test of the delta dynamics, the extended AMD is applied to (p,p') reactions at $E_{\rm lab}=800$ MeV for a ^{12}C target. It is found that the ratio and the absolute values for delta peak and quasielastic peak (QEP) in the $^{12}C(p,p')$ reaction are reproduced for angles $\Theta_{\rm lab} \gtrsim 40°$. For forward angles the QEP is overestimated, but generally the agreement between AMD calculations and experimental data is reasonable. The results of the AMD calculations are compared to one-step Monte Carlo (OSMC) calculations and a detailed analysis of multi-step and delta potential effects is given. Along this analysis a decomposition of the cross section into various reaction channels is presented and the reaction dynamics is discussed in detail. As important side results we present a way to apply a Galilei invariant theory for (N,N') reactions up to $E_{\rm lab} \approx 800$ MeV which ensures approximate Lorentz invariance and we discuss how to fix the width parameter ν of the single particle momentum distribution for outgoing nucleons in the AMD calculation.

PACS number(s): 25.40.Ep, 02.70.Ns, 14.20.Gk, 24.10.Cn

I. INTRODUCTION

In the interesting and expanding field of heavy ion physics several models for the treatment of the reaction dynamics have been developed. Especially microscopic transport models which take nuclear mean field effects and two-particle collisions into account have been very successful in explaining various kinds of experimental data. These models are extensions of the basic intranuclear model (INC) [1,2] in which two-nucleon collisions are taken into account, but the nuclear mean field is not treated self-consistently.

Two major microscopic approaches are used: transport models of the Boltzmann-Uehling-Uhlenbeck (BUU or VUU) type for the nuclear phase-space distribution function, solving either a nonrelativistic transport equation (nonrelativistic BUU) [3,5,4] or a relativistic transport equation (RBUU) [6] and the quantum molecular dynamics (QMD) [7] or its relativistic version (RQMD) [8], in which the nuclear phase-space distribution function is modeled by the sum of single-nucleon Gaussian wave packets, whose peak positions are propagated in time according to the many-body Newton equation, taking into account the self-consistent mean field as the sum of all two-body potentials.

In this paper we will discuss especially the antisymmetrized molecular dynamics (AMD) [9] which is an extension of the QMD and is similar to the fermionic molecular dynamics (FMD) proposed by Feldmeier [10]. In the AMD the nuclear wave function is assumed to be a Slater determinant of single-nucleon Gaussian wave packets. Other than in the FMD the Gaussian width parameter is time independent and, in addition to the pure mean field dynamics which is treated in the FMD, the two-nucleon collision process has been incorporated in the AMD [9].

The AMD has proved to be very successful in describing heavy ion collisions at medium energies ($\lesssim$200 MeV/nucleon) [9,11–16]. Because the AMD describes the total system with a Slater determinant of nucleon wave packets it has quantum mechanical character, which has been demonstrated in the ability of treating shell effects in the dynamical formation of fragments. Furthermore it has been shown that ground state wave functions of colliding nuclei given by the AMD are realistic and reproduce many spectroscopic data very well [17–20].

Since the AMD is successful for energies below 200 MeV/nucleon we want to apply it also at higher energies. Besides the question of Lorentz invariance, which we will also comment on in this paper, the opening of inelastic channels, i.e., the excitation of delta degrees of freedom, in the elementary nucleon-nucleon collision process is the most important effect for $E_{\rm lab}/A \gtrsim 600$ MeV. Therefore the first part of this paper is concerned with the question how to incorporate these inelastic channels into the AMD framework.

Before applying the extended AMD to heavy ion reactions we want to get a good understanding of the basic dynamics in our model. We choose to investigate (p,p') reactions at delta resonance energies. This is in the spirit of the research done by Engel *et al.* [21] who studied the pion-nucleus reaction to get a better understanding of the pion and delta dynamics in the BUU model. Another reason to apply the extended AMD to (p,p') reactions is that we found in a previous paper [22] that the AMD can reproduce data for (p,p') reactions for energies up to 200 MeV very well, so

*Present address: Advanced Science Research Center, Japan Atomic Energy Research Institute, Tokai-mura, Ibaraki-ken 319-11, Japan.

†Present address: Cyclotron Laboratory, Institute of Physical and Chemical Research (RIKEN), Hirosawa, Wako-shi, Saitama-ken 351-01, Japan.

we want to see if this is also true for higher energies.

One major field of interest concerning the (p,p') reaction is the shift of the delta peak in respect to the position in the (p,n) reaction and in respect to the position in the free case [23]. Experimentally it was found that in the (p,n) reaction the delta peak is shifted by 70 MeV in respect to the free case, whereby 40 MeV of the shift can be explained by the Fermi motion of the nucleons in the nucleus. We will discuss in this paper why in the calculated $^{12}C(p,p')$ reaction no shift of the delta peak can be observed. In the extended AMD, explained in this paper, the delta peak of (p,n) and (p,p') reaction are not shifted in respect to each other. Delta-hole correlations, which are believed to cause the additional 30 MeV shift not caused by Fermi motion (see above), have to be included into the model. Disregarding this open problem we will discuss the effect of the delta mean field on the delta peak position in the (p,p') reaction.

Finally to get a better understanding of the rather elaborated AMD calculation for the (p,p') reaction and the experimental data we compare to a one-step Monte Carlo (OSMC) simulation for this process. Thereby we can study the influence and importance of mean field effects, multistep processes, and Lorentz invariant kinematics.

The organization of this paper is as follows: In Sec. II we explain the AMD framework, discussing the introduction of delta degrees of freedom in the mean field and in the collision part; i.e., the delta potential and $NN \rightarrow N\Delta$ cross sections are introduced. In this section we also discuss the first calculations of delta separation energies of "delta nuclei" in the AMD. In Sec. III we give a description of the OSMC which we use for comparison with the AMD calculations. As an important basis for the studies presented in this paper, we study the question of Lorentz invariance for the (p,p') reaction within the OSMC. We find and show the interesting result, that a combination of Lorentz transformation from the laboratory frame into the total equal-velocity frame, Galilei invariant treatment in the equal-velocity frame, and following Lorentz back transformation into the laboratory frame ensures approximate Lorentz invariant results for energies around $E_{\rm lab} \approx 800$ MeV. In Sec. IV we discuss the results of AMD and OSMC in several steps and compare them with one another and with experimental data. First we present the results of the OSMC calculations and compare them with experimental data. Before we discuss the improvements which are achieved by the full AMD calculation, we explain how to fix all the parameters, especially the width parameter ν in the single-particle momentum distribution of the outgoing nucleons, in the AMD cross section calculation independent of the experiment. This is an important point of the calculation and should be understood well. After a detailed discussion of the multistep contributions to the cross section in the AMD calculation we proceed to discuss multistep and potential effects by comparing OSMC and AMD calculation with one another. In a final step we discuss dependence on the delta potential, on elastic nucleon-nucleon cross section, and on target momentum distribution of the calculations, and possible improvements of the AMD calculations. In Sec. V we give the summary and an outlook on what should or what could be done in future.

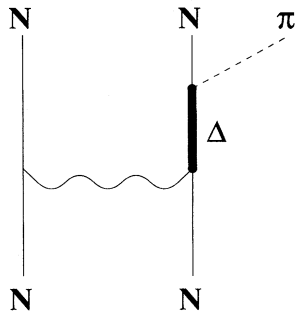

FIG. 1. Basic Feynman diagram for pion production in nucleon-nucleon collisions.

II. FORMULATION OF EXTENDED AMD

A. Basic idea

For intermediate energy collisions $E_{\rm lab}A \gtrsim 600$ MeV inelastic channels open in the elementary nucleon-nucleon process. The first channel to open is the pion production. As it is known from one-boson exchange model calculations for the elementary process $NN \rightarrow NN\pi$ [24,25] the pion production proceeds mainly through excitations of delta states as it is depicted in the Feynman diagram in Fig. 1. Diagrams with an excitation of an off-shell nucleon are only important for energies near the pion production threshold.

To include additional processes in the collision part of microscopic models the cross sections for these processes are needed. In the pion production case these cross sections are well known from experiment, but still there are in principle two ways to include pion production into microscopic models. One way is to treat the $NN \rightarrow NN\pi$ reaction directly, but this approach has several deficiencies. First of all the pions in heavy ion collisions are produced in the nuclear medium and therefore can be reabsorbed during the collision. Since the pion absorption process in the nucleus is not well understood, it is not clear how to treat it after a pion production in the nuclear medium. Salcedo *et al.* [26] calculated density-dependent pion absorption probabilities in the nucleus, but these calculations are based on a local Thomas-Fermi approximation and therefore are only valid for ground state nuclei and cannot be used in heavy ion collisions. Another drawback of the pure pion and nucleon cascade approach is that it is well known from experiment that also delta degrees of freedom survive in the nuclear medium.

Due to this drawback we choose another way which is also adopted in other microscopic models (see, for example, Refs. [1,8,27,28]). We cut the $NN \rightarrow NN\pi$ reaction into two steps: (1) $NN \rightarrow N\Delta$ and (2) $\Delta \rightarrow N\pi$ reaction. This is possible since the decay of deltas into pions occupies nearly 100% of the delta width.

To simulate the produced pion and nucleon momentum spectra correctly we have to take a mass distribution of the intermediate excited delta resonance into account. The origin of this mass distribution is easily understood by calculating the contribution of the Feynman diagram in Fig. 1 to the pion production cross section. In the production cross section a term proportional to the square of the delta propagator

$$G_\Delta \sim \frac{1}{M^2-[M_\Delta - i\Gamma(M)/2]^2} \tag{1}$$

will appear, where M^2 is the square of the four momentum of the delta, M_Δ the delta rest mass and $\Gamma(M)$ the width of the delta [see Eq. (15)]. Therefore off-shell states will contribute to the cross section with the weight of a M-dependent factor proportional to G_Δ^2. To simulate the off-shell character of the delta in microscopic models we populate delta states with a mass distribution proportional to G_Δ^2, interpreting M as the mass of the delta, but propagating the delta states as on-shell particles (see Sec. II D).

Now by including also the reverse processes $N\Delta \rightarrow NN$ and $\pi N \rightarrow \Delta$ we get a consistent picture of the delta and pion dynamics in heavy ion collisions. Unlike in the pure pion case discussed above, the pion absorption process is fixed in this approach, namely, (1) $\pi N \rightarrow \Delta$ and (2) $N\Delta \rightarrow NN$ lead to a pion absorption. It has been shown that this treatment of the collision term can reproduce many experimental data for the pion-nucleus reactions quite well [21]. Also unlike in the pure pion case the delta is included explicitly as degree of freedom.

As a first step of extending the AMD we discuss in this paper only the extension to include delta degrees of freedom. We expect that for calculations of (p,p') reactions for light targets the treatment of only delta degrees of freedom is sufficient due the following reasons. First, we find that the number of $\Delta N \rightarrow NN$ reactions is negligible even with infinite lifetime of the delta resonances and therefore the decay of the deltas with finite lifetime would not change the nucleon dynamics. Second, the reabsorption of the pions from decaying deltas does not change the outgoing proton momenta. That is, the momenta of protons originating from second generation deltas are small and hence do not show up in the calculated experimental data. In addition the pion reabsorption is expected to be small due to the size of the ^{12}C nucleus.

The decay of the deltas is calculated in the final time step of the calculation, when the deltas have escaped the nuclear medium (see Sec. II E). Later we plan to include also pion degrees of freedom in the nuclear medium and the full pion dynamics as explained above.

Besides the inclusion of the delta in the collision part it also has to be included into the mean field part of the theory. Normally this is done by treating the delta as a heavy nucleon and propagating it in the same mean field as the one for nucleons. More refined calculations have been done which use different mean potentials for deltas and nucleons [29]. We also adopted a delta potential which is different from the nucleon potential.

We will proceed in Sec. II B by explaining how to describe a system of deltas and nucleons in AMD, presenting the basic formulas, and also the various potentials used in the later calculations. After this we describe in Sec. II D the adopted cross sections, i.e., the delta related cross sections, and how we treat the collision term in the extended AMD.

B. Mean field with delta

The details of the AMD formulation have been explained in Ref. [9]. We will only comment on the modifications due to the introduction of delta degrees of freedom and those points which are important for the understanding of the calculation discussed in Sec. IV.

In AMD, the wave function of an A-nucleon system is described by a Slater determinant $|\Phi(Z)\rangle$,

$$|\Phi(Z)\rangle = \frac{1}{\sqrt{A!}} \det[\varphi_j(k)], \quad \varphi_j = \phi_{\mathbf{Z}_j}\chi_{\alpha_j}, \tag{2}$$

where χ stands for the spin-isospin function and α_j represents the spin-isospin label of the jth single-particle state, $\alpha_j = p\uparrow$, $p\downarrow$, $n\uparrow$, or $n\downarrow$. $\phi_{\mathbf{Z}_j}$ is the spatial wave function of the jth single-particle state which is a Gaussian wave packet,

$$\langle \mathbf{r}|\phi_{\mathbf{Z}_j}\rangle = \left(\frac{2\nu}{\pi}\right)^{3/4} \exp\left[-\nu\left(\mathbf{r}-\frac{\mathbf{Z}_j}{\sqrt{\nu}}\right)^2 + \frac{1}{2}\mathbf{Z}_j^2\right],$$

$$\mathbf{Z}_j = \sqrt{\nu}\mathbf{D}_j + \frac{i}{2\hbar\sqrt{\nu}}\mathbf{K}_j, \tag{3}$$

where the width parameter ν is treated as time independent in the present work. We take $\nu = 0.16\ \mathrm{fm}^{-2}$ in the calculation in this paper. Here $\mathbf{Z}_j$ is the complex vector whose real and imaginary parts, $\mathbf{D}_j$ and $\mathbf{K}_j$, are the spatial and momentum centers of the packet, respectively.

For the description of delta states we extend the possible number of spin-isospin functions χ in Eq. (2). This leads to the introduction of 16 additional states. But since we only use spin-independent cross sections and a spin-independent delta potential we can reduce the number of delta states to four,

$$\alpha_j^\Delta = \Delta^{++}, \Delta^+, \Delta^0, \Delta^-, \tag{4}$$

or in other words we use a delta spin averaged wave function. For deltas we use the same spatial wave functions as for nucleons as given in Eq. (3) leaving also the width parameter ν unchanged.

In the same way as in the original AMD the time development of the coordinate parameters, $Z = \{\mathbf{Z}_j (j=1,2,\ldots,A)\}$, due to mean field propagation is determined by the time-dependent variational principle,

$$\delta \int_{t_1}^{t_2} dt \frac{\langle \Phi(Z)|[i\hbar\,(d/dt) - H]|\Phi(Z)\rangle}{\langle \Phi(Z)|\Phi(Z)\rangle} = 0, \tag{5}$$

which leads to the equation of motion for Z,

$$i\hbar \sum_{j\tau} C_{k\sigma,j\tau} \frac{d}{dt} Z_{j\tau} = \frac{\partial}{\partial Z_{k\sigma}^*} \frac{\langle \Phi(Z)|H|\Phi(Z)\rangle}{\langle \Phi(Z)|\Phi(Z)\rangle},$$

$$C_{k\sigma,j\tau} \equiv \frac{\partial^2}{\partial Z_{k\sigma}^* \partial Z_{j\tau}} \ln\langle \Phi(Z)|\Phi(Z)\rangle, \tag{6}$$

where $\sigma,\tau = x,y,z$.

In the case of the extended AMD the many-body Hamiltonian has to be changed. For an A-body system with N_N nucleons and N_Δ deltas ($A = N_N + N_\Delta$) the Hamiltonian is given by

$$H=T+V$$
$$=\sum_{i_N=1}^{N_N}\frac{\mathbf{p}_{i_N}^2}{2m}+\sum_{i_\Delta=1}^{N_\Delta}\frac{\mathbf{p}_{i_\Delta}^2}{2m_{i_\Delta}}+\sum_{i_N<j_N}^{N_N}v_{NN}(i_N,j_N) \quad (7)$$
$$+\sum_{i_N}^{N_N}\sum_{i_\Delta}^{N_\Delta}v_{N\Delta}(i_N,i_\Delta)+\sum_{i_\Delta<j_\Delta}^{N_\Delta}v_{\Delta\Delta}(i_\Delta,j_\Delta).$$

It is a sum of kinetic energies for deltas and nucleons and the various two-body potentials for nucleon-nucleon, nucleon-delta, and delta-delta interactions.

During the dynamical reaction stage of the collision, the total system can be separated into several isolated nucleons and fragments. Since the wave functions of the center-of-mass motion of these isolated nucleons and fragments are Gaussian wave packets, each of these isolated particles carries spurious zero-point energy of its center-of-mass motion. The total amount of the spurious energy of center-of-mass motion can be expressed as a function of Z, [9,12] which we denote as $E_{\rm sprs}(Z)$. The actual Hamiltonian we use in the above equation of motion [Eq. (6)] is therefore given by $\langle\Phi(Z)|H|\Phi(Z)\rangle/\langle\Phi(Z)|\Phi(Z)\rangle-E_{\rm sprs}(Z)$.

As discussed in Sec. II A the deltas in the AMD will have a different mass than the free on-shell mass. This is reflected in Eq. (7) by using m_{i_Δ} in the expression for the kinetic energy.

Equation (6) with definitions Eqs. (7) and (2) are the basic formula for the extended AMD on behalf of the mean field, but to do actual calculations the form of the potentials have to be fixed.

For the effective two-nucleon force we adopt the Gogny force [30] which has been successfully used in studying heavy ion reactions with AMD [12,13]. The Gogny force consists of finite-range two-body force and density-dependent zero-range repulsive force. This force gives a momentum-dependent mean field which reproduces well the observed energy dependence of the nucleon optical potential up to about 200 MeV but levels off to be zero at higher energies whereas the experimental value at $E_{\rm lab}=$ 800 MeV is repulsive by about 50 MeV. The nuclear matter EOS given by Gogny force is soft with the incompressibility $K=$ 228 MeV. Corresponding to the choice of the Gogny force, the calculational formula of the total spurious center-of-mass energy $E_{\rm sprs}(Z)$ is taken to be the same as Ref. [12]. The binding energies of ^{12}C are calculated to be 92.6 MeV while the observed value is 92.2 MeV. The calculated rms radii of ^{12}C is 2.55 fm which is reasonable.

For the delta-nucleon potential we use a zero-range Skyrme-type force dependent on nucleon density (ρ_N),

$$v_{N\Delta}(\mathbf{r}_N,\mathbf{r}_\Delta)=\delta(\mathbf{r}_N-\mathbf{r}_\Delta)[t_{0\Delta}+t_{3\Delta}\rho_N^{\tau-1}(\mathbf{r}_N)] \quad (8)$$

with parameters $t_{0\Delta}$, $t_{3\Delta}$, and τ. This ansatz leads to a total delta-nucleus energy

$$V_\Delta=\langle\Phi(Z)|\sum_{i_N}^{N_N}\sum_{i_\Delta}^{N_\Delta}v_{N\Delta}(i_N,i_\Delta)|\Phi(Z)\rangle\Big/\langle\Phi(Z)|\Phi(Z)\rangle \quad (9)$$
$$=\int d\mathbf{r}\rho_\Delta(\mathbf{r})[t_{0\Delta}\rho_N(\mathbf{r})+t_{3\Delta}\rho_N(\mathbf{r})^\tau], \quad (10)$$

where ρ_N and ρ_Δ are the nucleon density and delta density, respectively. If we take the limit of infinite homgeneous nuclear matter of Eq. (10), we get the same form of the delta potential derived from the delta hole model by Ehehalt *et al.* in Ref. [29]. Therefore we use their parameters, $t_{0\Delta}=-700$ MeV fm^3, $t_{3\Delta}=$ 1750 MeV fm^5, and $\tau=5/3$ in the calculation. The parameters are chosen to reproduce the mean field value for the delta potential $U_\Delta(\rho_0)=\partial V_\Delta(\rho_0)/\partial\rho_\Delta=-30$ MeV for infinite nuclear matter, since this value is known from pion-nucleus scattering [31].

It is important to note that the nucleon-nucleon potential we use has finite range which leads to a momentum-dependent nucleon-nucleus potential. On the other side the delta-nucleon potential adopted here has zero range, and therefore the delta-nucleus potential is momentum independent.

Since there is nothing known about the delta-delta potential we choose $v_{\Delta,\Delta}$ to be zero. As a remark we want to point out that the calculation presented in this paper is independent of the choice of the delta-delta potential because in the calculated nucleon-nucleus reactions there is a maximum of one delta excited at a time. For the future calculation of heavy ion collisions we propose to use a delta-delta potential of the same type as the delta-nucleon potential Eq. (8) since these potentials should be similar except for spin-isospin factors and this choice gives a consistent picture of the interaction.

Numerically the integrations in Eq. (10) to calculate $V_\Delta(|\Phi(\mathbf{Z})\rangle)$ and those needed to get its derivatives due to $\mathbf{Z}_i$ are calculated in a similar way as those described in the Appendix A of [11] for the density-dependent part of the nucleon-nucleon interaction.

We also include the Coulomb potential in our calculation, but the results are not sensitive to this.

C. Delta nuclei

To construct the ground states of colliding nuclei in the AMD the frictional cooling method [17–20] is used which leads to a consistent picture of mean field dynamics and ground state nuclei. It has been checked that wave functions given by AMD are realistic and reproduce many spectroscopic data very well.

As the first check of the incorporated delta mean field dynamics we calculated the binding energies of "delta nuclei." This is in a way an academic study since no "delta nuclei" exist or can be detected, but it gives us information on the kind of wave functions we can have in a delta-nucleus system. In the future this kind of wave function could be used for studying the admixture of delta states in ground state wave function [32].

We calculated the delta separation energies for delta nuclei. For this we used the frictional cooling method to cool

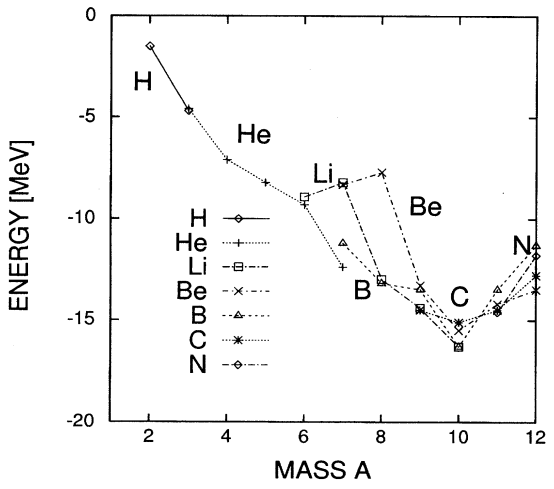

FIG. 2. Delta binding energies for various nuclei calculated in AMD with frictional cooling method.

first an ensemble of protons, neutrons, and one additional delta. Then we cooled the same ensemble of nucleons without the delta. The difference of the minimum energies of these two calculations gives the delta separation energy. The results for delta separation energies with the parameters given in Sec. II B are shown in Fig. 2.

The results in Fig. 2 can be understood in the following way: The delta separation energy is determined by the overlap between the delta Gaussian wave function and the residual many-nucleon system, as can be seen in Eq. (10). Therefore the minimum energy state calculated with the frictional cooling method leads to a delta state with maximum overlap with the nucleons. Because of the 3/2 isospin nature of the delta the configuration of maximum overlap is Pauli allowed. The mass dependence we get in Fig. 2 for the delta separation energy reflects the structure of the ground state wave function in AMD, which was able to describe the alpha clustering of light nuclei. We found that the delta separation energies for ^{4}He and ^{8}Be are the same. This can be understood on the basis of the two-alpha clustering of the ^{8}Be ground state. In the ground states of both nuclei the delta is in the middle of an alpha cluster, since this is the state of maximum overlap of delta and nucleus wave functions. Therefore they have the same delta separation energy. Because of the dissolving of the alpha structure and the existence of larger zones with higher nuclear densities for heavier masses, also the delta separation energies increase for heavier masses.

D. Deltas in the collision term

The idea of how to incorporate delta resonances in the collision part of microscopic theories was already discussed in Sec. II A. Here we give the cross sections adopted in the AMD. To include the deltas in the collision term we used the same cross sections as described in [21,28], therefore we will only recall the most important formulas.

1. $NN \rightarrow N\Delta$ reaction

The cross sections for the $NN \rightarrow N\Delta$ reaction are derived from the VerWest-Arndt parametrization for pion production cross sections in Ref. [33]. Assuming that all pions in the $NN \rightarrow NN\pi$ reaction are produced via a delta resonance we get

$$\begin{aligned}
&p+p \rightarrow n+\Delta^{++} && \sigma_{10}+1/2\sigma_{11},\\
&p+p \rightarrow p+\Delta^{+} && 3/2\sigma_{11},\\
&n+p \rightarrow p+\Delta^{0} && 1/2\sigma_{11}+1/4\sigma_{10},\\
&n+p \rightarrow n+\Delta^{+} && 1/2\sigma 11+1/4\sigma 10,\\
&n+n \rightarrow p+\Delta^{-} && \sigma_{10}+1/2\sigma_{11},\\
&n+n \rightarrow n+\Delta^{0} && 3/2\sigma_{11},
\end{aligned} \tag{11}$$

for the $NN \rightarrow N\Delta$ cross sections where σ_{if} denotes the cross sections used in the VerWest-Arndt parametrization for given isospin (f) and (i) of the final and initial nucleons, respectively [33]. The angular dependence of the $NN \rightarrow N\Delta$ is chosen in the same way as in Ref. [28].

As discussed in Sec. II A it is not enough to define the cross section for the $NN \rightarrow N\Delta$ reaction but we also need to use an appropriate mass distribution for the delta resonance. We choose

$$\frac{d\sigma_{NN\rightarrow N\Delta}}{dM^2} = \sigma_{NN\rightarrow N\Delta}\frac{F(M^2)}{\int_{(m_N+m_\pi)^2}^{(\sqrt{s}-m_N)^2} F(M^2)dM^2}, \tag{12}$$

$$F(M^2) = \frac{1}{\pi}\frac{M_\Delta \Gamma(M)}{(M^2-M_\Delta^2)^2+M_\Delta^2\Gamma(M)^2} \tag{13}$$

$$\approx \frac{1}{\pi M_\Delta}\frac{\Gamma(M)/4}{(M-M_\Delta)^2+\Gamma(M)^2/4} \tag{14}$$

with the delta rest mass $M_\Delta = 1232$ MeV and the momentum-dependent delta width [34]

$$\Gamma(M) = \left(\frac{q}{q_r}\right)^3 \frac{M_\Delta}{M}\left(\frac{v(q)}{v(q_r)}\right)^2 \Gamma_r \tag{15}$$

with

$$v(q) = \frac{\beta^2}{\beta^2+q^2},$$

$$\Gamma_r = 110 \text{ MeV},$$

$$\beta = 300 \text{ MeV},$$

where q and q_r denote the pion momentum in the rest frame of the delta for delta mass M and on-shell mass $M = M_\Delta$, respectively, defined as

$$q^2(M) = \frac{[M^2-(m_N-m_\pi)^2][M^2-(m_N+m_\pi)^2]}{4M^2}. \tag{16}$$

To get information on the validity of the adopted delta mass distribution we calculated the neutron momentum spectrum in the $p(p,n)p\pi^+$ reaction and compared to the experi-

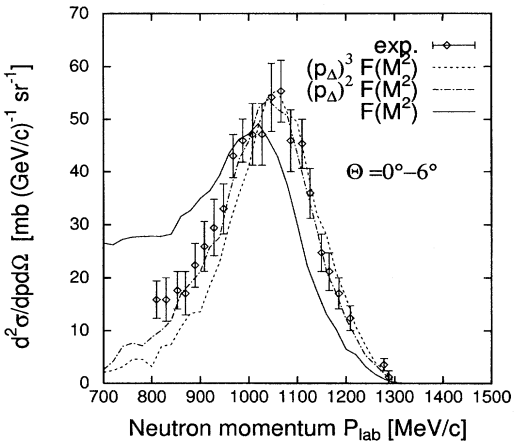

FIG. 3. OSMC of the $p(p,n)p\pi^+$ process at $E_{lab}=830$ MeV with different delta mass distributions. Experimental data are from Ref. [35]. (See text for details.)

mental shape of the spectrum. In Fig. 3 the result of this calculation is shown. The experimental data are a measurement of the neutron spectrum for laboratory angles $\Theta_n=0°-6°$ in coincidence with a proton and a π^+ for proton energy $E_{lab}=830$ MeV [35]. This reaction proceeds mainly via an excitation of a Δ^{++} state. The calculations which are shown were made with OSMC explained in detail in Sec. III using a proton target: A delta excitation in a proton-proton collision is simulated choosing the mass and momentum according to the given mass distribution [Eq. (14)] and the scattering angle according to the differential cross section of Ref. [28], respectively, by a Monte Carlo method. The deltas are assumed to decay isotropicly in their rest frame. Taking into account the proper transformations of the momenta we calculate the cross section for neutrons emitted in coincidence with a π^+ and a proton.

Besides the calculation with the mass distribution of Eq. (14) we made calculations with a mass distribution multiplied by a phase-space factor

$$f_{\text{phase space}}(M)=\left(\frac{p_\Delta(M)}{p_\Delta(M)^{\max}}\right)^n \tag{17}$$

with

$$p_\Delta^2(M)=\frac{[s-(m_N-M)^2][s-(m_N+M)^2]}{4s}, \tag{18}$$

where s is the square of the four-momentum of the system. $p_\Delta(M)$ is the momentum of the delta and $p_\Delta(M)^{\max}$ is the possible maximum momentum of the delta assumed for $M=m_n+m_\pi$. With this phase space factor [Eq. (17)] we take into account the fact that the final phase space for maximum delta mass, $M=\sqrt{s}-m_N$, is zero. In Fig. 3 calculations for the $p(p,n)p\pi^+$ reaction with $n=0$, $n=2$, and $n=3$ in Eq. (17) are shown. All calculations are scaled with the same factor to reproduce the experimental data. By taking into account only the mass distribution without a phase-space suppression factor, $n=0$, solid line, we find that the neutron spectrum is not reproduced so well. Too many heavy Δ^{++} with, consequently, low momentum neutron partners are formed in proton-proton collisions. Therefore the neutron momentum spectrum is shifted to lower energies. On the other hand using a strong suppression factor, $n=3$, leads to an underestimation of low momentum neutrons as seen in Fig. 3 (dashed line). The best fit for the neutron spectrum in the $p(p,n)p\pi^+$ reaction with the OSMC simulation is attained when using $n=2$ in Eq. (17) for the suppression factor as seen in Fig. 3 (dash-dotted line). Both low and high neutron momenta can be described rather well. In Sec. IV A we will comment on the dependence of the (p,p') reaction on the choice of the mass distribution.

2. $N\Delta\rightarrow NN$ reaction

Since there is no delta beam or delta target available the cross section for the $\Delta N\rightarrow NN$ process has to be derived by theory. It has been pointed out by several authors [36,37,21] that the naive detailed balance formula is not appropriate for this process. The simple argument to understand this point is that in the nucleon-nucleon collisions in which the deltas are formed the cross section has to be folded with the mass distribution to get the mass of the delta in the simulation, as described in Sec. II D 1, but in the $N\Delta\rightarrow NN$ reaction the delta in the simulation has a definite mass and therefore the mass distribution is not present for the calculation of the $N\Delta\rightarrow NN$ cross section. For a more detailed discussion of this problem see Ref. [21].

For simplicity we adopted the formula derived by Wolf *et al.* [37], which was proven to give a realistic description of the $N\Delta\rightarrow NN$ cross section (see discussion in Ref. [21]). Therefore we use

$$\sigma_{n\Delta^{++}\rightarrow pp}=\frac{1}{4}\frac{p_N^2}{p_\Delta^2}\sigma_{pp\rightarrow n\Delta^{++}}\frac{\int_{(m_N+m_\pi)^2}^{\infty}F(M^2)dM^2}{\int_{(m_N+m_\pi)^2}^{(\sqrt{s}-m_N)^2}F(M^2)dM^2} \tag{19}$$

with the $\sigma_{NN\rightarrow N\Delta}$ cross sections from VerWest-Arndt and the mass distribution $F(M^2)$ given in Eq. (14). In Eq. (19) p_Δ and p_N are the initial delta and the final nucleon momenta in the center-of-mass (c.m.) frame, respectively, whereas the factor 1/4 is due to spin averaging and a symmetry factor for identical particles in the final state. Since this cross section [Eq. (19)] is infinite for zero-energy collisions we apply a low momentum cutoff of $\sigma^{\max}=100$ mb, which takes the screening of the delta in the nuclear medium into account. This screening cutoff which is mainly introduced to cut the divergence of the cross section at low relative momenta can be physically motivated by the fact that the delta inside the nuclear medium can only interact with its neighbors and not with all nucleons. In case of the (p,p') reaction the screening is not effective because the produced deltas are fast deltas.

3. NN elastic scattering

For the nucleon-nucleon elastic scattering we used a new parametrization of Cugnon which is isospin dependent and therefore takes into account proton-neutron and proton-proton collisions differently [38]. This is not the case in the

old isospin-independent Cugnon parametrization [1], which is mainly adopted in other microscopic models, in which all isospin channels are treated the same way, in contrast to experiment. The isospin-dependent parametrization also includes a backward peak for the proton-neutron scattering which is not included in the isospin-independent parametrization.

E. Simulation

The actual simulation of the AMD is done in several steps. In the first step the ground states of the target and projectile nuclei are calculated by the frictional cooling method. With these ground state configurations the collision is calculated in the c.m. frame (see discussion about Lorentz invariant scattering in Sec. III B) using the above described cross sections and mean fields for the particles. The delta decay is not yet incorporated in the AMD therefore deltas will survive until the final state of the calculation. The decay of these deltas is calculated assuming an isotropic decay in the rest frame of the delta. In this step the relativistic expression for the pion energy is used. In the final step the statistical decay of primordial formed fragments is calculated. Primordial fragments mean the fragments which are present when the dynamical stage of the reaction has finished. These fragments are not in their ground states but are excited, and they decay through evaporation with a long time scale. In this paper, the switching time from the dynamical stage to the evaporation stage was chosen to be 150 fm/c. Before the statistical decay calculation we calculate the decay of the remaining deltas. Statistical decays of fragments were calculated with the code of Ref. [39] which is similar to the code of Pühlhofer [40].

F. Calculation of cross section

The experimental data we want to compare with in this paper are given in the laboratory frame. As discussed in Sec. III B we choose a combination of Lorentz and Galilei transformation to achieve approximate Lorentz invariance using a Galilei invariant theory. The combinations of transformations have to be also taken into account for the cross section calculation. In the equal-velocity frame the Galilei invariant expression of the double-differential cross section has the following form:

$$\frac{d^2\sigma}{d\Omega dp}=\int_0^\infty 2\pi b db\,\frac{d^2\mathcal{N}(\mathbf{p},b)}{d\Omega dp},$$

$$\frac{d^2\mathcal{N}(\mathbf{p},b)}{d\Omega dp}d\Omega dp=\left\langle \sum_{\substack{i=\text{isolated}\\ \text{protons}}}\rho_i(\mathbf{p})\right\rangle_b d^3p, \tag{20}$$

$$\rho_i(\mathbf{p})=|\langle \mathbf{p}|\phi_{\mathbf{Z}_i}\rangle|^2=\left(\frac{1}{2\pi\hbar^2\nu}\right)^{3/2}\exp\left[-\frac{1}{2\hbar^2\nu}(\mathbf{p}-\mathbf{K}_i)^2\right], \tag{21}$$

where $d^3p=p^2dpd\Omega$ and $\langle\rangle_b$ stands for the average value over the events with impact parameter b. In this formula, the outcoming protons are expressed by Gaussian wave packets with momentum width $\hbar\sqrt{\nu}$.

Applying the Lorentz transformation into the laboratory frame we get

$$\frac{d^2\sigma}{d\Omega' dp'}=\int_0^\infty 2\pi b db\left\langle \sum_{\substack{i=\text{isolated}\\ \text{protons}}}\rho_i'(\mathbf{p}')\right\rangle_b p'^2 \tag{22}$$

with

$$\rho_i'(\mathbf{p}')=\rho_i(\mathbf{p})\frac{E}{E'}, \tag{23}$$

where $\mathbf{p}$ and E are the relativistic expressions for the momentum and the energy in the equal-velocity frame, $\mathbf{p}'$ and E' the relativistic momentum and energy in the laboratory frame and $\rho_i(\mathbf{p})$ the function given in Eq. (21).

III. ONE-STEP MONTE CARLO SIMULATION FOR (p,p')

A. Formulation

In order to get a better understanding of the rather elaborate AMD calculations, we also perform one-step Monte Carlo (OSMC) simulations of the (p,p') reaction. In this section we explain the OSMC simulation. In the OSMC simulation the summation over the impact parameter $\int 2\pi b db$ is not made for simplicity. The projectile protons are initialized in the laboratory frame according to the relativistic momentum energy relation. Since we studied the influence of the target momentum distribution on the results for the (p,p') reaction we initialized different target momentum distributions. As one approach we attributed a random momentum smaller than the Fermi momentum at normal nuclear density $|\mathbf{p}|<|\mathbf{k_f}|$ to the nucleons. As another approach we used the local Thomas-Fermi ansatz to simulate the momentum distribution by first choosing a position in coordinate space according to the space density

$$\rho(r)=\rho_0\left[1+\alpha\left(\frac{r}{a}\right)^2\right]\exp\left[-\left(\frac{r}{a}\right)^2\right], \tag{24}$$

which is based on the harmonic-oscillator model, with parameters $\alpha=1.247$ and $a=1.649$ fm for the ^{12}C target determined through experiment [41]. And then we attributed randomly a momentum smaller than the local Fermi momentum, which gave us the momentum distribution $f(p)$,

$$f(p)=\int_0^\infty dr\,4\pi r^2\rho(r)\frac{\Theta[k_f(r)-p]}{4\pi/3[k_f(r)]^3},$$

$$k_f(r)=\left(\frac{3\pi^2}{2}\rho(r)\right)^{1/3}, \tag{25}$$

where $\Theta(x)$ is the step function; $\Theta(x)=1$ for $x>0$, $\Theta(x)=0$ for $x<0$.

As next step we transform the energy and the momentum of the projectile proton from the laboratory frame into the equal-velocity frame of target and projectile with Lorentz transformation. The transformation β for the incident proton in the z direction and a target with A nucleons with four-momenta

$$\mathbf{p}_\mu=\{E_p,0,0,p_z\}, \tag{26}$$

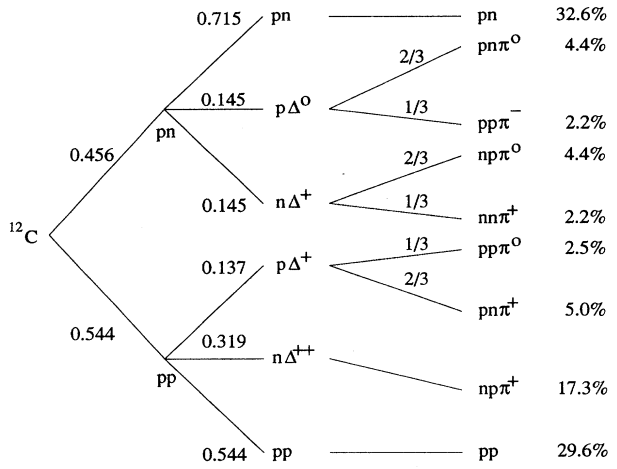

FIG. 4. The total reaction probabilities in the OSMC simulation which are determined by the total cross sections for proton incident energy $E_{\rm lab}=800$ MeV.

$$\mathbf{p}_{\mu}^{\mathbf{A}}=\{Am_n,0,0,0\} \tag{27}$$

into the equal-velocity frame with condition

$$\frac{p_z'}{E_p'}=-\frac{p_z'A}{E_A'} \tag{28}$$

is

$$\{\beta_x,\beta_y,\beta_z\}=\left\{0,0,\frac{E_p}{p_z}-\sqrt{\left(\frac{E_p}{p_z}\right)^2-1}\right\}, \tag{29}$$

where A is the number of target nucleons and m_n the nucleon mass. It can be seen that this transformation is not dependent on the number of target nucleons. This is natural since the total equal-velocity frame is the same as the two-nucleon c.m. frame, if we disregard the Fermi motion of the target nucleons.

We choose to transform into the total equal-velocity frame, because in this frame nonrelativistic approximations can be applied. In the equal-velocity frame we change to nonrelativistic kinematics using the obtained momenta and the nonrelativistic expression for the energy. Also for the transformation of the target nucleon momenta into the equal-velocity frame we use the nonrelativistic Galilei transformation. In the next section it will be shown that this kinematical treatment of the scattering, which we also adopt in the AMD, leads to approximate Lorentz invariance.

The two-nucleon collision in OSMC is calculated in the c.m. frame of the two nucleons with Galilei invariant kinematics. As possible collision processes we incorporated delta excitation and elastic scattering. We fixed the ratio of delta excitation to elastic events beforehand, which is well justified, since this ratio is mainly determined by the initial energy of the proton. The cross section ratios for $E_{\rm lab}=800$ MeV which are incorporated in the calculation are given in Fig. 4.

In the case of a delta event we have to determine the mass of the delta and, since we take into account the charge of the particles, the charge of the delta. The charge and mass are chosen according to the ratio given by the cross sections and the mass distribution in Sec. II D 1, respectively. To calculate the cross sections the $\sqrt{s}$ of the two-nucleon system is needed. This we calculate in the two nucleon Galilei c.m. frame using the nonrelativistic expression for the energies. In the next section the validity of this evaluation is discussed.

The three-momentum of the outgoing particles, deltas, or nucleons, are determined according to the angle-dependent cross sections in the two-nucleon c.m. by the Monte Carlo method. Since in the delta excitation kinetic energy is transformed into mass energy the final relative momentum in the c.m. frame for the $NN\rightarrow N\Delta$ reaction decreases.

The decay of the excited deltas is calculated in the delta rest frame assuming an isotropic decay. For the delta decay we use a Lorentz invariant prescription because the pions are light particles and need to be treated in relativistic invariant kinematics. It is important to mention here that the Lorentz transformation in the delta decay is only adopted to transform from the delta rest frame to the equal-velocity frame of the total system. The charge of the pions and nucleons is chosen according the probabilities given by the Clebsch Gordan coefficients for the decay.

To calculate the multiplicity distribution of the outgoing protons or neutrons in the laboratory frame for given momenta and angle, the momenta of the particles are backtransformed from the total equal-velocity frame to the laboratory frame by Lorentz transformation with $\beta_{\rm back}=-\beta$ given in Eq. (29). The multiplicity distributions are calculated with the formula

$$\frac{d^2N}{dp_i d\Omega_i}=\frac{N_i}{\Delta p 2\pi\Delta\cos\Theta N_{tp}}, \tag{30}$$

where N_i is the number of nucleons with momentum $p_i-\Delta p/2\leq p\leq p_i+\Delta p/2$ and $\cos\Theta_i-\Delta\cos\Theta/2\leq\cos\Theta_i\leq\cos\Theta_i+\Delta\cos\Theta/2$, and N_{tp} the number of performed simulations. In the calculations shown we use $\Delta p=0.02$ GeV and $\Delta\Theta=2.99°$. In the calculation of cross sections for the (p,p') reaction we use a factor $X_{\rm factor}$ to scale to the experimental data:

$$\frac{d^2\sigma}{dp_i d\Omega_i}=\frac{d^2N}{dp_i d\Omega_i}X_{\rm factor}. \tag{31}$$

The factor $X_{\rm factor}$ has a dimension, which is because we do not integrate over the impact parameter. The number of simulations was varied according to the accuracy needed.

B. Lorentz invariance

To justify the approach used for the scattering kinematics in the OSMC simulations and also the AMD calculations we compared the OSMC simulation described in Sec. III A with simulations using pure Galilei and pure Lorentz invariant kinematics, respectively. For this comparison we did one-step elastic scattering simulations using an isotropic angular distribution for the scattering in the nucleon-nucleon c.m. frame disregarding the charges of the particles. The results for the multiplicity distribution for Lorentz invariant kine-

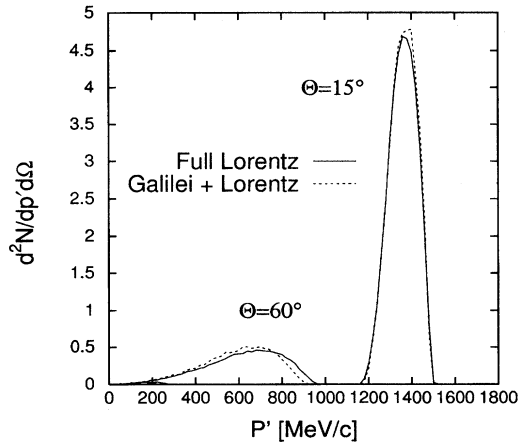

FIG. 5. One-step scattering simulation for the quasielastic process for $\Theta = 15°$ and $\Theta = 60°$ at $E_{\rm lab} = 800$ MeV with full Lorentz invariant kinematics (solid line) and combination of Galilei and Lorentz invariant kinematics (OSMC) (dashed line). (See text for details.)

matics and OSMC simulations are shown in Fig. 5. The momentum of the target nucleons is chosen randomly between zero and the Fermi momentum $k_f = 270$ MeV. The calculations shown are for $E_{\rm lab} = 800$ MeV and scattering momenta in the laboratory frame. We show calculations for laboratory angles $\Theta = 15°$ and $\Theta = 60°$. The solid line represents results with the Lorentz invariant kinematics and the dashed line results with the OSMC. The results agree very well with each other. In Fig. 6 the results of Lorentz invariant calculations (solid line) are compared with Galilei invariant scattering calculations. Again the calculations were performed for laboratory angles $\Theta = 15°$ and $\Theta = 60°$. The Galilei invariant calculations differ significantly from the Lorentz invariant results. We did calculations starting with correct relativistic energy (dashed line in Fig. 6), and correct relativistic momentum (dash-dotted line in Fig. 6). Both calculations deviate strongly from the correct relativistic calculation (solid line in Fig. 6).

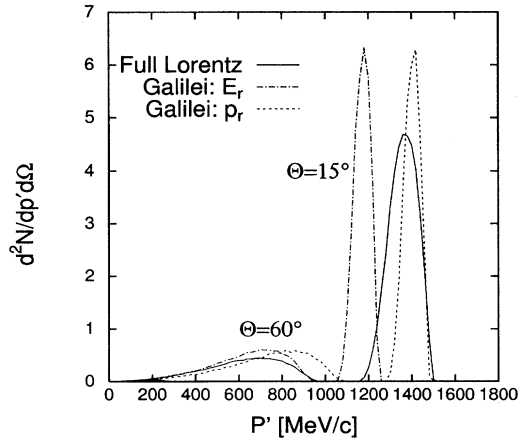

FIG. 6. One-step scattering simulation for the quasi elastic process for $\Theta = 15°$ and $\Theta = 60°$ at $E_{\rm lab} = 800$ MeV with full Lorentz invariant kinematics (solid line) and Galilei invariant kinematics starting with correct energy (dashed dotted line) and correct momentum (dashed line). (See text for details.)

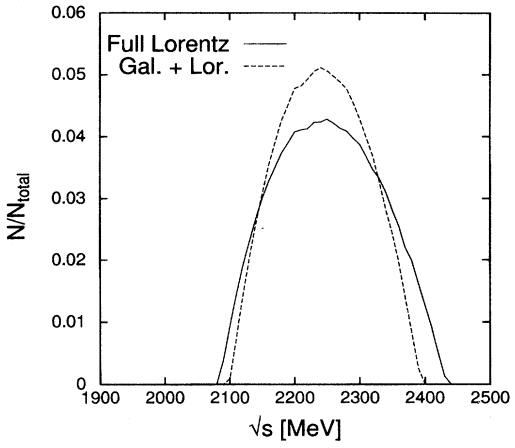

FIG. 7. The distribution of $\sqrt{s}$ in one-step scattering calculations at $E_{\rm lab} = 800$ MeV with full Lorentz invariant kinematics (solid line) and combination of Galilei and Lorentz invariant kinematics (OSMC dashed line). (See text for details.)

To show that the two-nucleon $\sqrt{s}$ distribution used in the OSMC simulation and the AMD agrees with the relativistic prescription we compared the $\sqrt{s}$ distributions of the OSMC and the Lorentz invariant scattering. Again there are only small differences for the resulting $\sqrt{s}$ distribution as seen in Fig. 7: OSMC simulation (dashed line), Lorentz invariant kinematics (solid line). The averaged deviation of $\sqrt{s}$ is less than 1% and, since the elastic and inelastic nucleon-nucleon cross sections in the considered energy region have a smooth dependence on $\sqrt{s}$, the difference between OSMC and purely Lorentz invariant kinematics is not important.

IV. COMPARISON WITH EXPERIMENT

As first step to understand the employed delta dynamics in AMD we have calculated the inelastic scattering of protons on light nuclei. We have compared the calculation with experimental data in which both the delta excitation and the quasielastic peak (QEP) are prominent. In the following discussion we will see that behind the seemingly easy to understand experimental data complicated and interesting processes are hidden.

A. One-step Monte Carlo calculations

First we want to discuss the results of the OSMC calculations. The total reaction probabilities for the (p,p') reaction for $E_{\rm lab} = 800$ MeV incorporated in the OSMC are shown in Fig. 4. The ratio between inelastic to elastic cross section is approximately 2 to 3, which points out that inelastic channels are very important for this energy region. Deviations from the total reaction probabilities in the differential cross sections discussed in the following are due to the anisotropic cross sections used in the OSMC and due to kinematical reasons.

In Fig. 8 we show the OSMC calculations (solid line) for the (p,p') reaction at $E_{\rm lab} = 800$ MeV for laboratory angles

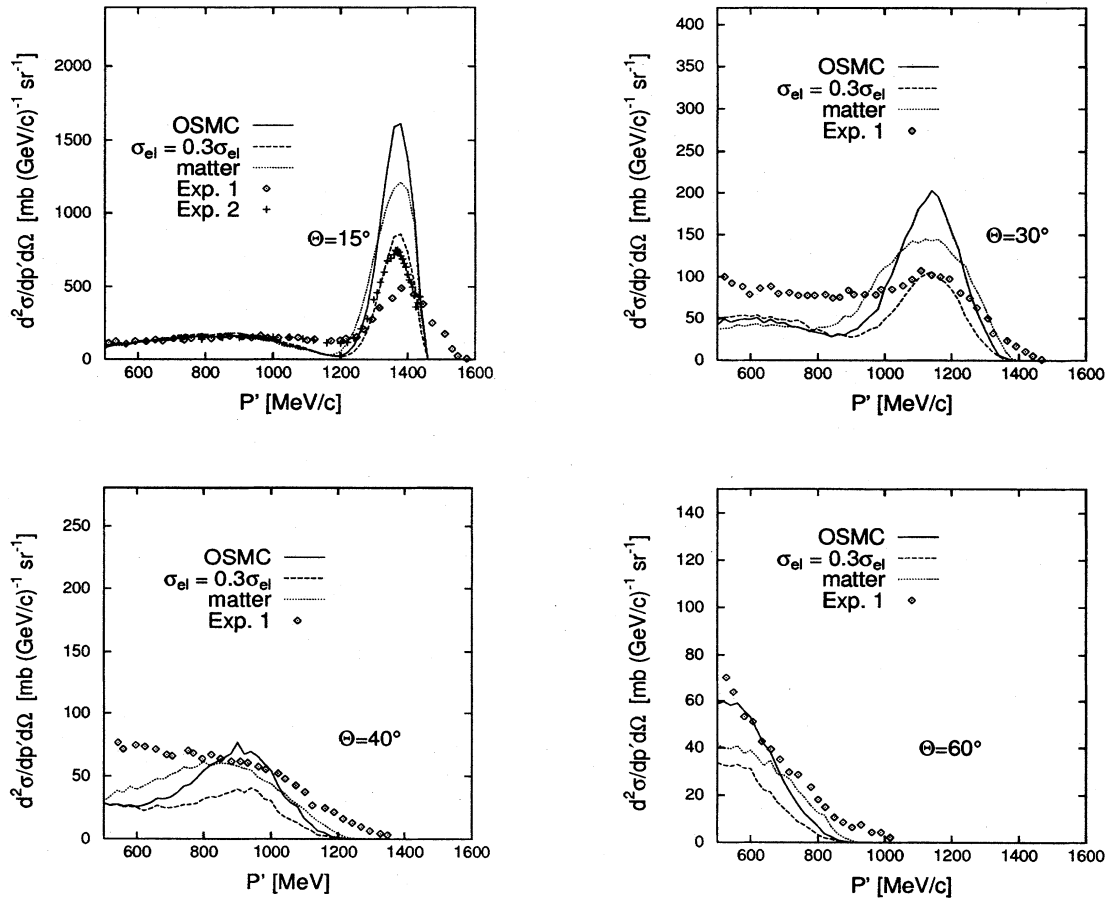

FIG. 8. OSMC calculations described in Sec. III in comparison with experimental data for $d^2\sigma/d\Omega/dp'$ in $^{12}C(p,p')$ reactions for various angles $\Theta=15°$, 30°, 40°, and 60° in the laboratory system and $E_{lab}=800$ MeV. Calculations are for free elastic nucleon-nucleon cross section (solid line), 70% reduced elastic nucleon-nucleon cross section (dashed line) and box momentum distribution for the target (dotted line). For the solid and dashed lines the Thomas-Fermi momentum distribution for the target is used, and for the dotted line free elastic nucleon-nucleon cross section is used. (See text for details.) Experimental data are from Ref. [42] (diamonds) and Ref. [45] (plusses).

$\Theta=15°$, 30°, 40° and $\Theta=60°$. In the experimental data for $\Theta=15°$ the QEP can be clearly seen and the contribution of inelastic or multistep scattering to the cross section is well separated. In Fig. 8 we show two different experimental data for $\Theta=15°$ (see Refs. [42,45]), which differ only in the QEP region. This difference is claimed to be due to the resolution of the experimental apparatus [42]. We scale the OSMC calculation to reproduce the momentum region $p'=600$–800 MeV at $\Theta=15°$. To achieve this, we have to use $X_{factor}=260$ mb which is larger than the measured total cross section (209 mb for $E_{lab}=860$ MeV in Ref. [43] and 229 mb for $E_{lab}=553$ MeV in Ref. [44]).

We find that in the OSMC calculation the QEP for $\Theta=15°$ is largely overestimated and for $\Theta=30°$ and $\Theta=40°$ the QEP is much more pronounced than in the experimental data. The high momentum tail in the experimental data at $\Theta=15°$ is physically not allowed and consequently cannot be reproduced.

For $\Theta=30°$,40° and $\Theta=60°$ there is an underestimation of the low and high momentum tail of the cross section in the shown momentum region. The underestimation is especially strong in the momentum region $p'=500$–800 MeV for $\Theta=30°$ and $p'=500$–700 MeV for $\Theta=40°$. Another defect of the OSMC calculation is that the flat behavior of the cross section for $p'=1000$–1200 MeV at $\Theta=15°$ is not reproduced. Instead there is a dip in the calculated cross section.

B. AMD calculations

Before discussing the results of the AMD calculation we have to comment on the cross section calculation in AMD for the (p,p') reaction. A straightforward approach leads to Eq. (22) for the double-differential cross section. This formula is based on the assumption that every nucleon in AMD has the same width ν, but this is not true for all nucleons in the (p,p') reaction. For example it is obvious that the incoming proton has a definite energy and therefore zero-momentum width ν. Therefore the role of the width parameter has to be reconsidered. Concerning the width parameter ν in the AMD, we recall, that the width parameter ν in the AMD is important for reproducing the total density and momentum distribution of ground state nuclei. In the collision prescription in the present version of the AMD (see Ref.

[11]), only the Gaussian distribution in the coordinate space is taken into account, whereas in the momentum space only the centers of Gaussian wave packets are used. Therefore in nucleon-nucleus collision calculation with AMD the momentum distribution of the target is only partly explored dynamically. For heavy ion reactions the effect of the high momentum tail of the wave function is negligible as long as subthreshold processes are not important for the calculated process, but, as will become clear in the following, the QEP region of the (p,p') reaction is sensitive to the width parameter ν of the outgoing nucleons.

In order to solve the above-sketched problem, getting a reliable exploration of the momentum distribution of the target in the (p,p') reaction within the AMD calculation, two lines of argumentation can be followed. One is to take into account the Gaussian momentum distribution of the colliding nucleons in the collision prescription, and the other is to change the width parameter ν of the outgoing nucleons. In the first approach the width parameter ν of the incoming proton should be zero, at least in the simulation of the first nucleon-nucleon collision. Technically this can be taken into account in the collision prescription, but it is not clear what width should be attributed to the incoming proton after the first collision. We follow the second approach to get a reliable treatment of the momentum distribution of the target, since there is a way to determine the width ν of the outgoing nucleons independently of experimental data, namely, the AMD calculation should reproduce the width of the QEP caused by the Fermi motion. We do calculations both with the OSMC and a modified version of the AMD, the "one-step AMD" for the (p,p') reaction. In the case of the OSMC we use both, a box momentum distribution for the target, like in nuclear matter, and a Thomas-Fermi momentum distribution for the target, as explained in Sec. III A. In the one-step AMD calculation we allow only one possible collision in each event after which the particles propagate in their mean field. We determine the width ν of the outgoing nucleon so that the one-step AMD calculation reproduces the width of the QEP in the (p,p') reaction given by the OSMC calculation with the Thomas-Fermi momentum distribution for the target.

As can be seen in Fig 8, the QEP at $\Theta=15°$ is much narrower than at $\Theta=30°$. The width parameter ν in the one-step AMD calculation is fitted to reproduce the width of the QEP caused by the Fermi motion. In the actual calculations we do not change the width parameter ν but we use a cut of the Gaussian momentum distribution

$$\rho'(p)=0 \quad \text{for} \quad \left[\frac{1}{2\hbar^2\nu}(\mathbf{p}-\mathbf{K}_i)^2\right]>Q_{\text{cut}}, \tag{32}$$

and renormalize the function $\rho'(p)$ in Eq. (22), which has the same effect as adjusting the width parameter ν in the single-particle wave functions.

We find that in the one-step AMD calculation for the $^{12}C(p,p')$ reaction we have to use $Q_{\text{cut}}=0.5$ for $\Theta=15°$, $Q_{\text{cut}}=1.0$ for $\Theta=30°$, $Q_{\text{cut}}=1.6$ for $\Theta=40°$ and no cut for $\Theta=60°$ in order to reproduce the width of the QEP in the OSMC simulation with Thomas Fermi momentum distribution of the ^{12}C target. In all AMD calculations we use the above-determined cuts.

By comparing the one-step AMD with OSMC calculations with box momentum distribution, the nuclear matter case, we find that we only have to apply a cut at $\Theta=15°$ to reproduce the effect of the Fermi motion. This is a nice result which states that for cross section calculations for heavy ion collisions no cuts are needed, since a large amount of nuclear matter is involved in the reaction.

After fixing all parameters we can proceed to discuss the results of the AMD calculations which are shown in Fig. 9 (solid line). In general we find a better reproduction of the experimental data with the AMD than with the OSMC. Here we will only state the improvements established by using the AMD instead of the OSMC. In the following section (Sec. IV C) we study the reaction mechanism in the AMD calculation in detail and in Sec. IV D we will discuss the origin of the improvements in the AMD.

Instead of an underestimation of the low momentum region for angles $\Theta=30°$ and $\Theta=40°$ in the OSMC, we find that the experimental data can be better reproduced in the AMD calculation. In general the agreement with the experimental data for these angles is much better in the AMD than in OSMC, because the smooth behavior of the experimental data for $\Theta=30°$, and especially for $\Theta=40°$, is much better reproduced. In the case of the OSMC we do not get absolute cross sections and therefore the comparison of the calculations with the shape of the momentum (p') dependence is important and this is much better reproduced in the AMD calculations.

The AMD can also reproduce the high momentum tail of the cross section for $\Theta=30°$ better and for $\Theta=40°$ and for $\Theta=60°$ much better than the OSMC. Also the flat behavior of the cross section for $p'=1000$–1200 MeV at $\Theta=15°$ is reproduced.

So we find that the agreement between AMD calculation and experiment is much better than the one between OSMC and experiment. The experimental data can be quantitatively reproduced in AMD, whereby the elastic processes seem to be overestimated in forward direction. In Sec. IV E we will discuss how to improve the AMD results, but in the next sections we will first try to get a clearer understanding of the reaction dynamics in the AMD for the (p,p') reaction.

C. Multistep contributions to the cross section

To get a better understanding of the reaction dynamics we calculated the decomposition of the cross section into different multistep contributions and reaction processes. The result of this decomposition is shown in Fig. 10. We show calculations for four angles: $\Theta=15°,30°,40°$ and $\Theta=60°$. The elastic multistep contributions shown in Fig. 10 are protons with one-step elastic scattering [ELA-1 step, long-dashed line] and protons with two-step elastic scattering [ELA-2 step, dashed line]. Nucleons involved in inelastic collisions can contribute to two different sources of outgoing protons: protons emitted as delta decay products and protons which acted as collision partners in the delta excitation process. The contributions of these different sources in inelastic collisions are also shown in Fig. 10: Protons emitted as partner of an excited delta in the first chance collision [Δ-1 step(N), dotted

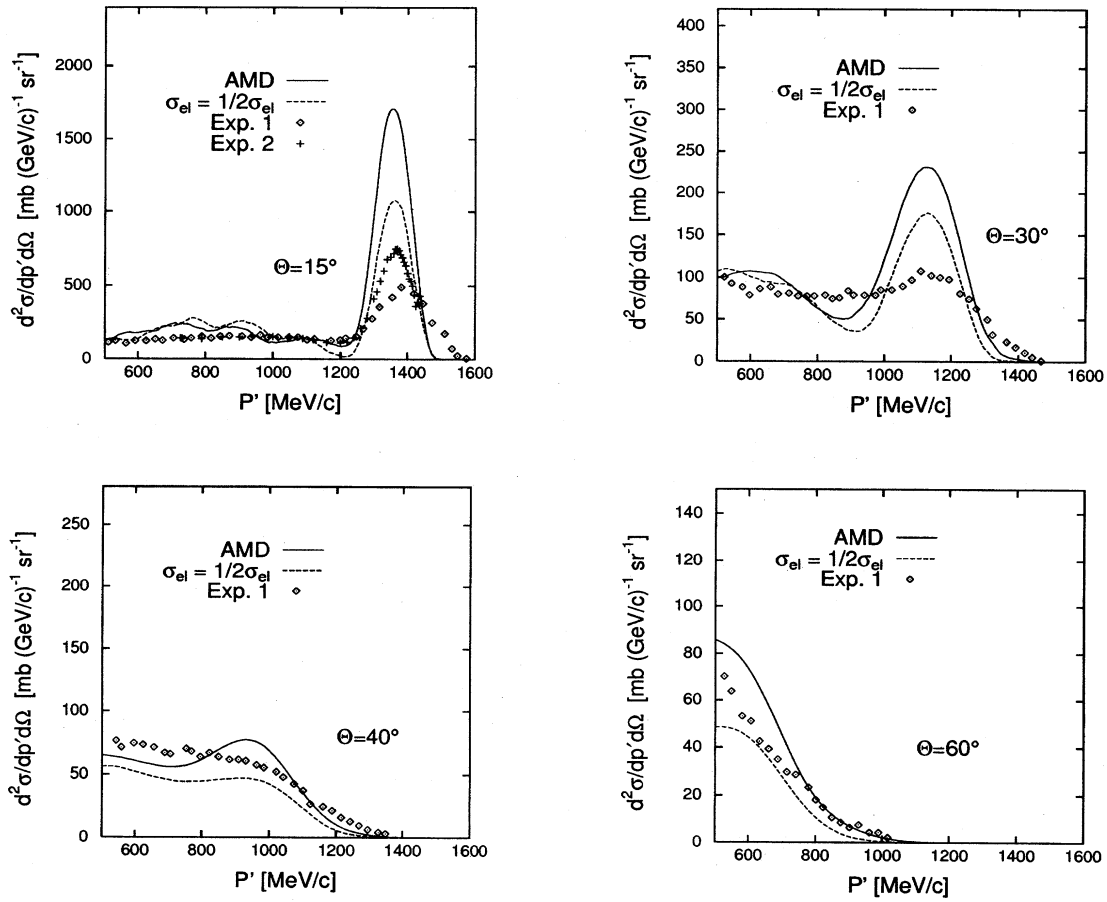

FIG. 9. AMD calculation with free elastic nucleon-nucleon cross section (solid line) and 50% reduced elastic nucleon-nucleon cross section (dashed line) in comparison with experimental data for $d^2\sigma/d\Omega/dp'$ in $^{12}C(p,p')$ reactions at $E_{lab}=800$ MeV. Experimental data are the same as in Fig. 8.

line], and protons from delta decay after the first chance collision [Δ-1 step(Δ), dash-dotted line].

In the calculation for $\Theta=15°$ we see that mainly the one-step scattering process (long-dashed line) contributes to the QEP. The two-step contribution is much smaller for all momenta. A similar behavior is found for $\Theta=30°$, where the two-step contribution (dashed line) gets more important but is smaller than the one-step contribution for almost all outgoing proton momenta. At $\Theta=30°$, $\Theta=40°$, and $\Theta=60°$ the two-step contributions dominate the high momentum tail of the proton spectrum, since one-step scattering cannot reach this region of the phase space easily.

For $\Theta=30°$ and $\Theta=40°$ we find that for the lower momentum part of the cross section, below the QEP, many higher step processes contribute to the cross section. Besides the processes shown in Fig. 10 two-step and three-step elastic processes followed by an inelastic process contribute to the cross section. Therefore the reproduction of the smooth behavior of the cross section in this momentum region is quite sensitive to the ratio of inelastic to elastic cross section and the multistep contributions.

D. Comparison of AMD and OSMC: Multistep and potential effects

After having discussed the reaction dynamics in the AMD in detail we can comment on the differences between AMD and OSMC and what kind of physical effects are important for the (p,p') reaction.

As one could have expected, the main differences of OSMC and AMD are due to multistep processes, but the details of the origins of the differences are much more interesting than this plain statement, and therefore we discuss this question in detail. Also we have to investigate the role of potential effects which could interfere with the multistep contribution effects. To make the above statements more transparent we show in Fig. 11 the outcome of the one-step AMD calculation (dashed line) we mentioned in Sec. IV B, in which we did not allow any more collisions after the first proton-nucleon collision occurred in the AMD, propagating the particles from this time step onwards only in their mean fields without collisions. Therefore the only difference be-

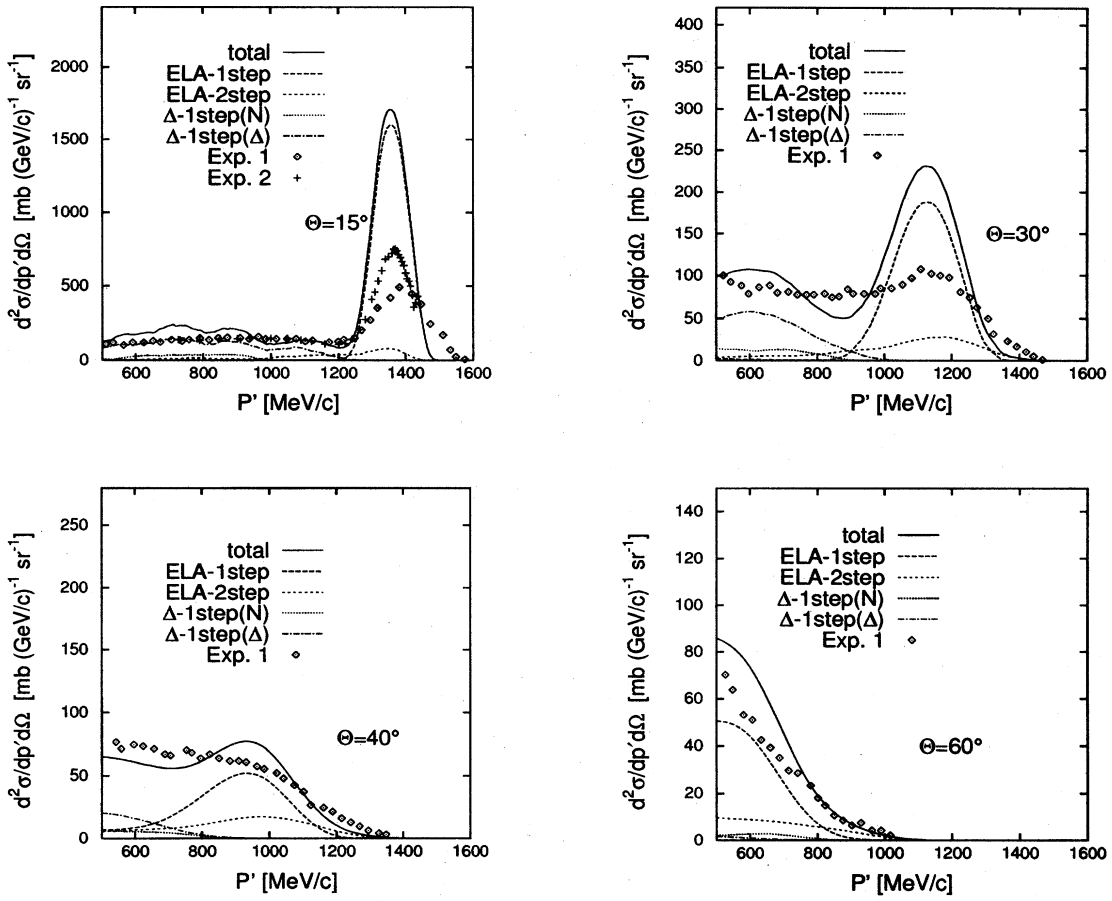

FIG. 10. Multistep decomposition of the original AMD calculation (solid line) given in Fig. 9. (See text for details.) Experimental data are the same as in Fig. 8.

tween one-step AMD and OSMC is the treatment of the mean fields in the AMD and the differences between one-step AMD and AMD are only due to multistep contributions. The results of the one-step AMD should not be confused with the one-step contributions to the full AMD calculations discussed in the last section.

First we want to discuss the differences due to multistep contributions and the improvements achieved by this in reproducing the experimental data with the AMD. Therefore we compare one-step AMD (dashed line) and AMD (solid line) calculations in Fig. 11 on the basis of the multistep decomposition of the AMD results shown in Fig. 10. Multistep contributions which involve at least one inelastic step are mainly responsible for a better reproduction of the experimental data for momentum below the QEP at $\Theta=30°$ and $\Theta=40°$ in the AMD calculation. The high momentum tails above the QEP at ($\Theta=30°$) $\Theta=40°$ and $\Theta=60°$ are better reproduced in the AMD due to multistep elastic scattering contributions.

The apparent quantitative agreement of the heights of the QEPs for $\Theta=30°$ and $\Theta=40°$ in the one-step AMD and the AMD is not a trivial result. The reduction of the QEP due to multistep scattering is balanced out by an enhancement due to multistep processes in the AMD. At $\Theta=60°$ multistep processes lead even to an increase of the cross section in the QEP region in the AMD calculations. For $\Theta=15°$ the net effect of multistep contributions is a reduction of the QEP.

Another important improvement of the AMD calculations due to multistep contributions is that the flat behavior of the experimental data at $\Theta=15°$ for momenta $p'=$ 1000–1200 MeV can be described unlike in the OSMC where there is a dip in the cross section.

Concerning the potential effects in AMD we find no significant difference between one-step AMD and OSMC calculations except of a shift of the QEP of 20 MeV/c to lower momenta at $\Theta=15°$. There are no apparent differences caused by the inclusion of potentials for the particles in the other areas of the phase space. (See more detailed discussion about delta potential effects in the next section.)

E. Dependence on delta potential, cross section and target momentum distribution, and improvements

Since we have now established a detailed understanding of the reaction dynamics in the AMD we can study the dependence of the results on the physical input quantities and what we can learn about these in the (p,p') reaction.

One important question which is always asked, but not yet well understood, is the question of the delta potential and the behavior of the delta in the nuclear medium. We want to

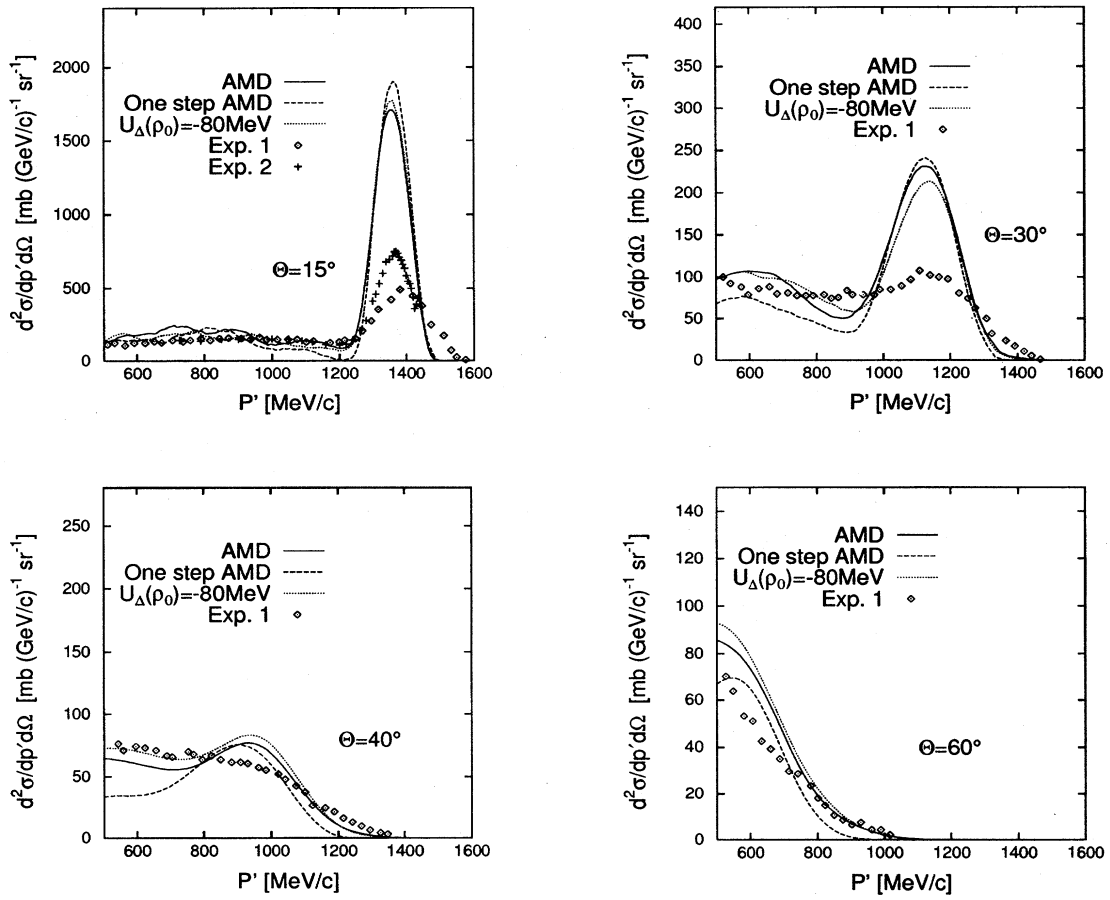

FIG. 11. Original AMD calculation (solid line), one-step AMD calculation (dashed line), and AMD calculation with shifted delta potential (dotted line) in comparison with experimental data for $d^2\sigma/d\Omega/dp'$ in $^{12}C(p,p')$ reactions at $E_{lab}=800$ MeV. (See text for details.) Experimental data are the same as in Fig. 8.

comment on this from the viewpoint of the AMD calculations made in this paper. In the previous section we stated that there is no apparent potential effect when comparing OSMC and AMD results, but here we will investigate the potential effects in more detail.

To study the effect of the delta potential we did calculation with a potential which has the same density dependence as the one in Eq. (8), but is shifted to reproduce $U_\Delta(\rho_0)=-80$ MeV. This choice of the potential is motivated by the following idea: We assume that the delta potential is momentum independent and has the original value $U_\Delta(\rho_0)=-30$ MeV. We recall here that we have not treated the momentum dependence of the nucleon potential correctly in the present version of the AMD and our nucleon potential at $E_{lab}=800$ MeV is $U_N(\rho_0)\approx 0$ MeV. If we used the correct value $U_N(\rho_0)\approx 50$ MeV, it would lead to the difference $U_N(\rho_0)-U_\Delta(\rho_0)\approx 80$ MeV. Hence using a delta potential with $U_\Delta(\rho_0)=-80$ MeV in the present version of the AMD leads to the desired value $U_N(\rho_0)-U_\Delta(\rho_0)\approx 80$ MeV.

The AMD calculations with shifted delta potential are shown in Fig. 11 (dotted line). There is no apparent difference between the calculations with different delta potentials. Only if we calculate the multistep decomposition of the cross section we find that the high momentum threshold of the one-step inelastic contributions are different for different delta potentials. But these differences cannot be seen in the sum of all contributions because in the high momentum threshold region for these processes their contributions to the cross sections are just a few mb and therefore are hidden below the multistep and elastic step contributions to the cross section. This is also the reason why we did not find any apparent potential effect in the previous section.

We point out at this point that the choice of the delta mass in the $NN\rightarrow N\Delta$ process is not treated fully self-consistent in the present version of the AMD. To determine the mass of the delta we use the delta mass distribution Eq. (13) dependent on the $\sqrt{s}$ of the initial nucleon-nucleon pair, but we do not take the effect of the delta potential on the delta mass distribution into account. This improvement should be made in future AMD calculations. Still the above findings about the influence of the delta potential on AMD calculations for experimental data for the $^{12}C(p,p')$ reaction would hold. This is due to the fact that in the inelastic threshold region (see argumentation above) where the change of the delta potential has the biggest effect, the multistep and elastic scattering dominates the cross section. To study the influence of the delta potential we have to compare with experimental data which are mainly dominated by the excitation of deltas,

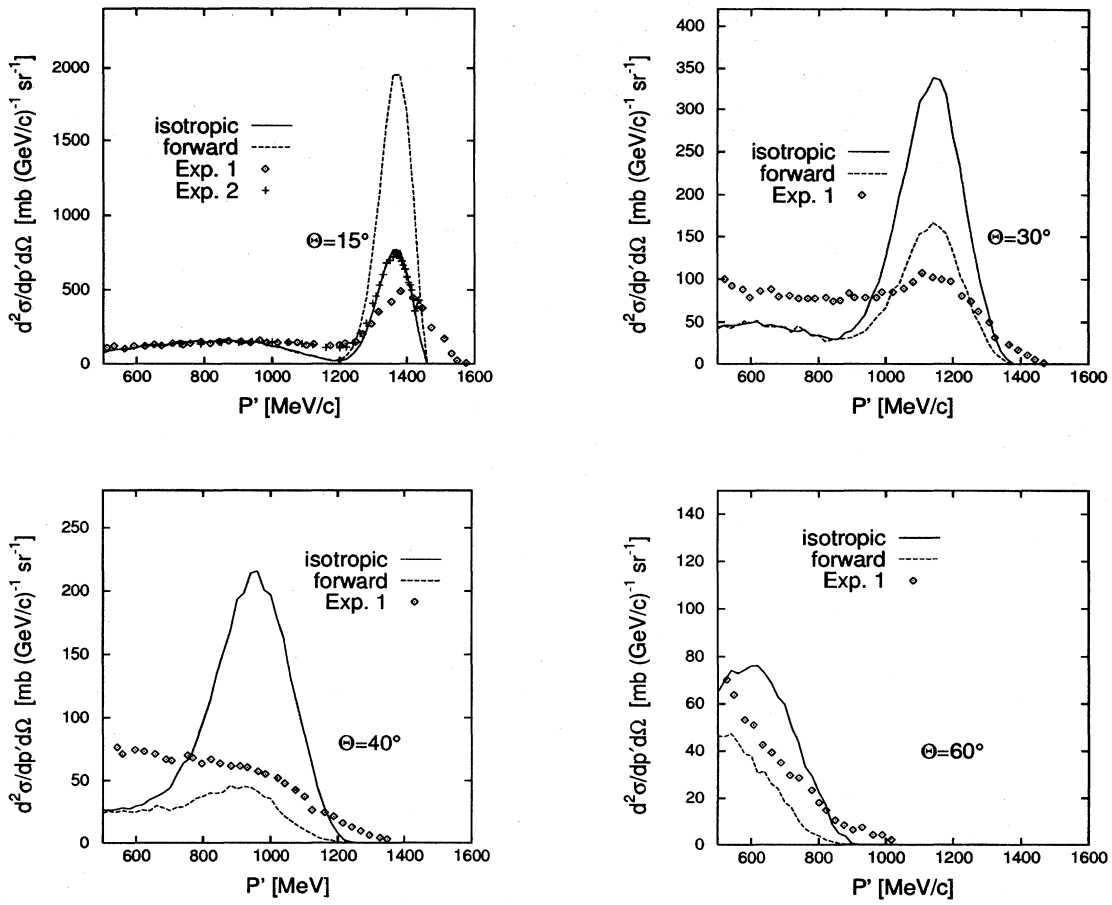

FIG. 12. OSMC calculation with isotropic nucleon-nucleon cross section (solid line), forward peaked nucleon-nucleon cross section (dashed line), and box momentum distribution for the target (dotted line) in comparison with experimental data for $d^2\sigma/d\Omega/dp'$ in ^{12}C (p,p') reactions at $E_{\text{lab}}=800$ MeV. (See text for details.) Experimental data are the same as in Fig. 8.

i.e., delta mass distribution from π + nucleon invariant mass spectra (see for example Ref. [35]) in $(p,x)x'\pi$ reactions.

Concerning the dependence on the angular distribution of the adopted elastic nucleon-nucleon cross section we find strong dependence on the adopted parametrization. Since the OSMC calculation is much less time consuming we studied the cross section dependence within the OSMC. In Fig. 12 we show the result of the OSMC calculation for isotropic elastic nucleon-nucleon cross section (solid line) and for the isospin-independent Cugnon parametrization [1] for the elastic nucleon-nucleon cross section. Since the isospin-independent Cugnon parametrization is strongly forward peaked for all nucleon-nucleon channels, at $\Theta=15°$ the QEP is largely overestimated and at larger angles the QEP is underestimated [Fig. 12 (dashed line)]. In case of an isotropic nucleon-nucleon cross section the opposite is the case: The QEP at $\Theta=15°$ is much better reproduced, but for all other angles there is a large overestimation of the QEP [Fig. 12 (solid line)].

If we would do AMD calculations with the isotropic or the isospin-independent parametrization of the nucleon-nucleon cross section, neither choice would improve the results, which we achieved using the isospin-dependent parametrization of Cugnon. This is a satisfying result, since the isospin-dependent parametrization of Cugnon gives the best reproduction of the experimental data for elastic nucleon-nucleon scattering among the discussed parametrizations.

The strong dependence on the angular distribution of the nucleon-nucleon cross section and the effect of multistep scattering discussed above show how difficult it is to explain the considered experimental data for the (p,p') reaction which at first view seem to be very dull, uninteresting and easy to understand.

With the OSMC we checked the dependence of the results on the adopted momentum distribution of the target. In Fig. 8, besides the original OSMC calculation (solid line), also calculations with a box momentum distribution of the target (dotted line) are shown. The higher momentum components in the target lead to a broadening and reduction of the QEP. But in general the (p,p') reaction is not sensitive to the details of the momentum distribution in the target. The large variation of width of the QEP between Thomas-Fermi and box momentum distributions is caused by a large difference of the distributions themselves.

We did calculations with different mass distributions for the delta discussed in Sec. II D, but these only have a minor effect on the result of the calculation.

We have checked the effect of Pauli blocking in the OSMC. All OSMC calculations presented in this paper in-

corporate Pauli blocking. In the AMD the Pauli blocking is incorporated naturally (see Ref. [11] for details). We found that only the high momentum tail of protons at $\Theta = 15°$ is influenced by the consideration of Pauli blocking.

In general we see in the multistep decomposition of the AMD calculation in Fig. 10 that the contribution of elastic scattering is overestimated. This is especially prominent for $\Theta = 30°$ but also for other angles the defect can be seen. As a first attempt to cure this problem we did calculations in which we reduced the elastic nucleon-nucleon cross section artificially by 50%. This leads to the results shown in Fig. 9 (dashed line). The QEP can be reproduced much better and also the general agreement between experimental data and AMD calculation gets better. At $\Theta = 40°$ the smooth momentum dependence of the cross section is well described but the cross section is slightly underestimated.

The reduction of the elastic cross section is also motivated by the fact that we find a total reaction cross section of 307 mb for the $^{12}C(p,p')$ reaction at $E_{lab} = 800$ MeV in the AMD calculation, which is too large compared to the experimental results (see Sec. IV A).

With the OSMC we did calculations with a 70% reduced elastic cross section. For this choice of the cross section we have to use $X_{factor} = 190$ mb which is less than the measured total cross section. The results are shown in Fig. 8 (dashed line). Also in case of the OSMC the reduction of the cross section leads to a better agreement with the experimental data for $\Theta = 15°$ and $\Theta = 30°$. But in the case $\Theta = 40°$ and $\Theta = 60°$ the agreement with the experimental data gets worse.

One possible physical effect which will lead to a reduction of elastic scattering events is the correct treatment of the momentum dependence of the mean field. As written above the adopted Gogny force does not give the correct momentum dependence of the nucleon-mean potential. Instead of $U_N(800\ \text{MeV}) \approx 50$ MeV the Gogny force leads to $V_N(800\ \text{MeV}) \approx 0$ MeV. Using a repulsive potential would lead to more nucleons diffracted to larger angles. This also implies that nucleons would have less interactions with the target since they are diffracted from their way through the target. This effect is especially true for nucleons with large impact parameter which contribute strongly to the elastic scattering peak. In a future investigation this idea should be tested.

Finally we briefly want to comment on the differences of the AMD and OSMC calculations for the $^{12}C(p,p')$ reaction at $E_{lab} = 800$ MeV from the PWIA calculations by Alexander *et al.* [46] for the same process. Alexander *et al.* take one-step elastic and one-step inelastic scattering into account. Unlike in the OSMC results discussed in this paper the smooth dependence on the outgoing proton momenta for larger angles can be better described in their PWIA calculation. This is because they use an unrealistic high pion production cross section. Therefore they need no multistep contributions to get the smooth behavior of the cross section for large angles as we find in the AMD calculations. If one would add the multistep contributions to their PWIA calculation this would lead to a large overestimation of the experimental data.

Another defect of the PWIA calculations of Alexander *et al.* is that they fit the heights of the QEP in the double-differential cross section with an angle-dependent scale factor which hides the strong dependence on the angular distribution of the elementary nucleon-nucleon cross section.

In the region of phase space where multistep contributions determine the cross section Alexander *et al.* underestimate the inelastic scattering cross section. This is in good agreement with the findings presented in this paper using the OSMC model.

V. SUMMARY

In this paper we discussed how to incorporate delta degrees of freedom into the AMD. We especially discussed the inclusion of inelastic channels in the collision term and the form of the delta-nucleon potential. For the delta-nucleon potential we used a Skyrme-type potential which gives $U_\Delta(\rho_0) \approx -30$ MeV for infinite nuclear matter calculation, thereby reproducing the experimental data found in pion-nucleus scattering.

With the help of the frictional cooling method we calculated delta separation energies for "delta nuclei." There we found that the minimum energy of the delta-nucleus system in the present calculation is achieved when the delta and nucleus wave functions are in the state of maximum overlap. Therefore we found that the clustering of the AMD wave function is reflected in the delta separation energy.

For a detailed discussion of the (p,p') reaction we developed a one-step Monte Carlo (OSMC) model for this reaction. As required by the energy region considered in this paper ($E_{lab} \approx 800$ MeV) we incorporated both nucleon and delta degrees of freedom using the same cross section as done in the AMD.

As a first application of the OSMC we investigated the question of Lorentz invariance for nucleon-nucleus scattering for energies $E_{lab} \approx 800$ MeV. We found the interesting result that, applying a combination of Lorentz transformations, a Galilei invariant theory can also be used to treat nucleon-nucleus scattering in this energy region. Also the calculation of $\sqrt{s}$ in a Galilei invariant theory can be performed in an approximate Lorentz invariant way.

Before applying the AMD calculation to the (p,p') reaction, we discussed how to determine the width parameter ν of the single-particle wave function for outgoing nucleons. The determination was made by comparing one-step AMD and OSMC calculations. This is a unique way to get parameter-independent results in the AMD.

Both with extended AMD and OSMC, we performed calculations of double differential cross sections $d\sigma^2/dp'/d\Omega$ for the $^{12}C(p,p')$ reaction for angle- and momentum-dependent cross sections. We found a quantitative difference between AMD and OSMC calculations which is mainly due to multistep contributions to the cross section, which are absent in one-step calculations.

Generally we find that OSMC and AMD can reproduce the qualitative behavior of the experimental data. Both the delta peak and the QEP can be seen in the calculation and the angle dependence of the cross section is reproduced rather well. In case of the AMD we find a quantitative good description of the experimental data except for the overestimation of the QEP in the forward direction. Therefore the agreement with the experimental data improves if we perform calculations with a reduced elastic cross section. One reason

for the reduced elastic cross section could be that the correct treatment of the momentum dependence of the nucleon mean field at this energy region leads to a repulsive potential and, because of this, to more diffraction of the incoming protons to larger angles. This then leads to less elastic scattering probability. This effect would be most serious for big impact parameters.

For a better understanding of the reaction process we performed a multistep decomposition of the cross section. To get the smooth momentum dependence seen in the experimental data for $\Theta = 30°$ and $\Theta = 40°$, a complicated interplay of elastic and inelastic channels is important which is approximately reproduced by the AMD calculation.

One interesting result of the multistep decomposition of the cross section is that two and higher step contributions govern the high momentum tail of cross sections for larger angles. The unsatisfying point is that an overall reduction of the elastic scattering cross section, which seems to be needed to reproduce the experimental data better, leads to an underestimation of multistep processes and therefore to an underestimation of the cross section in the region of phase space where these processes determine the cross section, such as the region of the high momentum tail at larger angles. Again the above-offered cure to the overestimation of the elastic scattering, a correct treatment of the momentum dependence of the mean field, would mainly reduce the one-step contributions and not the multistep contributions.

As one important physical property, which is often discussed but not well understood, we discussed the influence of the delta potential on the (p,p') reaction. We found that the results for the (p,p') reaction are not very sensitive to the choice of the delta potential. The reason for this is that the contributions to the cross section which change due to different delta potentials are small and are hidden below multistep and elastic step contributions to the cross section. We pointed out that the dependence on the delta potential will be more apparent in calculations for experimental data, where the excitation of the delta dominates the reaction, i.e., delta mass distribution from π + nucleon invariant mass spectra (see for example Ref. [35]).

Commenting on previous calculations we found that the AMD model gives a much more realistic picture of the $^{12}C(p,p')$ reaction at $E_{lab} = 800$ MeV than the PWIA calculations of Alexander *et al.* in Ref. [46] for the same process.

Finally we conclude with an outlook: This paper leaves many open questions and ways to extend the field of study. First of all a nucleon-nucleon potential should be adopted which gives the correct momentum dependence of the nucleon mean field and then the statements made about the change of the heights of the QEP should be tested.

Also the full pion dynamics should be incorporated in the AMD, which is expected to have a minor effect on the calculations presented in this paper where we treat a light target ^{12}C, since we find that the $\Delta N \rightarrow NN$ process is negligible. But for the study of the (p,p') reaction for heavier targets the correct treatment of pion absorption ($\Delta N \rightarrow NN$ reaction) and pion reabsorption ($\pi N \rightarrow \Delta$) will be much more important.

With fully incorporated pion dynamics detailed studies of pion production and pion-nucleus reactions can be done.

Another way to follow is to perform a more detailed study of dependence on delta and nucleon potential. Especially a momentum-dependent delta potential could be introduced and the difference between momentum-dependent and momentum-independent potentials could be discussed. For this investigation we have to compare to experimental data which are more sensitive to the adopted potentials. Also we have to introduce a self-consistent treatment of the delta mass in the AMD for the the $NN \rightarrow N\Delta$ process as discussed in Sec. IV E.

Further, (p,n) reactions should be investigated in detail with the AMD. For this study the question has to be discussed how to incorporate delta-hole correlations and how to describe the time development of these correlations in the AMD framework.

ACKNOWLEDGMENTS

One of us (A.E.) wants to thank the Japan Society for Promotion of Science for financial support for this project. We thank Dr. I. Tanihata and Dr. S. Ohta for their arrangements for using this computer system. Most of the calculations for this research project were performed with the Fujitsu VPP500 of RIKEN, Japan.

[1] J. Cugnon, T. Mizutani, and J. Vandermeulen, Nucl. Phys. **A352**, 505 (1981).

[2] J. Cugnon, D. Kinet, and J. Vandermeulen, Nucl. Phys. **A379**, 553 (1982).

[3] G. F. Bertsch and S. Das Gupta, Phys. Rep. **160**, 189 (1988).

[4] U. Mosel, Annu. Rev. Nucl. Part. Sci. **41**, 29 (1991).

[5] W. Cassing, V. Metag, U. Mosel, and K. Niita, Phys. Rep. **188**, 363 (1990).

[6] B. Blättel, V. Koch, W. Cassing, and U. Mosel, Phys. Rev. C **38**, 1767 (1988).

[7] J. Aichelin and H. Stöcker, Phys. Lett. B **176**, 14 (1986); J. Aichelin, Phys. Rep. **202**, 233 (1991); G. Peilert, H. Stöcker, W. Greiner, A. Rosenhauer, A. Bohnet, and J. Aichelin, Phys. Rev. C **39**, 1402 (1989).

[8] H. Sorge, H. Stöcker, and W. Greiner, Ann. Phys. (N.Y.) **192**, 266 (1989).

[9] A. Ono, H. Horiuchi, T. Maruyama, and A. Ohnishi, Phys. Rev. Lett. **68**, 2898 (1992); Prog. Theor. Phys. **87**, 1185 (1992).

[10] H. Feldmeier, Nucl. Phys. **A515**, 147 (1990); in *Proceedings of the NATO Advanced Study Institute on the Nuclear Equation of State*, Peñiscola, 1989, Vol. 216A of *NATO Advanced Study Institute Series B: Physics*, edited by W. Greiner and H. Stöcker (Plenum, New York 1989), p. 375; H. Feldmeier, K. Bieler, and J. Schnack, Nucl. Phys. **A586**, 493 (1995).

[11] A. Ono, H. Horiuchi, T. Maruyama, and A. Ohnishi, Phys. Rev. C **47**, 2652 (1993).

[12] A. Ono, H. Horiuchi, and T. Maruyama, Phys. Rev. C **48**, 2946 (1993).

[13] A. Ono and H. Horiuchi, Phys. Rev. C **51**, 299 (1995).
[14] H. Horiuchi, in *Proceedings of the NATO Advanced Study Institute on Hot and Dense Nuclear Matter*, Bodrum, 1993, Vol. 335 of *NATO Advanced Study-Institute Series B: Physics*, edited by W. Greiner, H. Stöcker, and A. Gallmann (Plenum, New York, 1994), p. 215.
[15] H. Horiuchi, in *Proceedings of the Fifth International Conference on Nucleus-Nucleus Collisions*, Taormina, 1994, edited by M. Di Toro, E. Migneco, and P. Piattelli [Nucl. Phys. **A583**, 297 (1995)].
[16] H. Horiuchi, A. Ono, and Y. Kanada-En'yo, in *Proceedings of the Seventh International Conference on Nuclear Reaction Mechanisms*, Varenna, 1994, edited by E. Gadioli [Ricerca Scientifica ed Educazione Permanente Supplemento No. 100, p. 421 (1994)].
[17] H. Horiuchi, in *Proceedings of the International Symposium in Honor of Akito Arima; Nuclear Physics in 1990's*, Santa Fe, 1990, edited by D. H. Feng, J. N. Ginocchio, T. Otsuka, and D. Strottman [Nucl. Phys. **A522**, 257c (1991)].
[18] H. Horiuchi, T. Maruyama, A. Ohnishi, and S. Yamaguchi, in *Proceedings of the International Conference on Nuclear and Atomic Clusters*, Turku, 1991, edited by M. Brenner, T. Lönnroth, and F. B. Malik (Springer, Berling, 1992), p. 512; in *Proceedings of the International Symposium on Structure and Reactions of Unstable Nuclei*, Niigata, 1991, edited by K. Ikeda and Y. Suzuki (World Scientific, Singapore, 1992), p.108.
[19] Y. Kanada-En'yo and H. Horiuchi, Prog. Theor. Phys. **93**, 115 (1995).
[20] H. Horiuchi, Y. Kanada-En'yo, and A. Ono, in *Proceedings of the Second Internationa Conference on Atomic and Nuclear Clusters*, Santorini, 1993, edited by G. S. Anagnostatos and W. von Oertzen [Z. Phys. A **349**, 279 (1994)].
[21] A. Engel, W. Cassing, U. Mosel, M. Schäfer, and Gy. Wolf, Nucl. Phys. **A572**, 657 (1994).
[22] E. I. Tanaka, A. Ono, H. Horiuchi, T. Maruyama, and A. Engel, Phys. Rev. C **52**, 316 (1995).
[23] F. Osterfeld, Rev. Mod. Phys. **64**, 491 (1992).
[24] B. J. VerWest, Phys. Lett. **83B**, 161 (1979).
[25] M. Schäfer, H. C. Dönges, A. Engel, and U. Mosel, Nucl. Phys. **A575**, 429 (1994).
[26] L. L. Salcedo, E. Oset, M. J. Vincente-Vacas, and C. Garcia-Regio, Nucl. Phys. **A484**, 557 (1988).
[27] J. J. Molitoris and H. Stöcker, Phys. Lett. B **162**, 47 (1985).
[28] Gy. Wolf, G. Batko, W. Cassing, U. Mosel, K. Niita, and M. Schäfer, Nucl. Phys. **A517**, 615 (1990).
[29] W. Ehehalt, W. Cassing, A. Engel, U. Mosel, and Gy. Wolf, Phys. Lett. B **298**, 31 (1993).
[30] J. Dechargé and D. Gogny, Phys. Rev. C **43**, 1568 (1980).
[31] Y. Horikawa, M. Thies, and F. Lenz, Nucl. Phys. **A345**, 386 (1980).
[32] A. I. Amelin, M. N. Behr, B. A. Chernyshev, M. G. Gornov, Yu. B. Gurov, S. V. Lapushkin, P. V. Morokhov, V. A. Pechkurov, R. R. Shafigullin, T. D. Shurenkova, V. P. Koptev, M. G. Ryskin, R. A. Eramzhiam, and K. O. Oganesian, Phys. Lett. B **337**, 261 (1994).
[33] B. J. VerWest and R. A. Arndt, Phys. Rev. C **25**, 1979 (1982).
[34] J. H. Koch, E. J. Moniz, and N. Ohtsuka, Ann. Phys. (N.Y.) **154**, 99 (1984).
[35] J. Chiba, T. Kobayashi, I. Arai, N. Kato, H. Kitayama, A. Manabe, M. Tanaka, K. Tomizawa, D. Beatty, G. Eduards, C. Glashausser, G. J. Kumbartzki, R. D. Ransome, and F. T. Baker, Phys. Rev. Lett. **67**, 1982 (1991).
[36] P. Danielewicz and G. F. Bertsch, Nucl. Phys. **A533**, 712 (1991).
[37] Gy. Wolf, W. Cassing and U. Mosel, Nucl. Phys. **A545**, 139c (1992); **A552**, 549 (1993).
[38] J. Cugnon, and M.-C. Lemaire, Nucl. Phys. **A489**, 781 (1988); private communication.
[39] T. Maruyama, A. Ono, A. Ohnishi, and H. Horiuchi, Prog. Theor. Phys. **87**, 1367 (1992).
[40] F. Pühlhofer, Nucl. Phys. **A280**, 267 (1977).
[41] C. W. de Jager, H. de Vries, and C. de Vries, At. Data Nucl. Data Tables, **14**, 479 (1974).
[42] I. Tanihata, S. Nagamiya, A. Schnetzler, and H. Steiner, Phys. Lett. **100B**, 121 (1982).
[43] F. F. Chen, C. P. Leavitt, and A. M. Shapiro, Phys. Rev. **99**, 857 (1955).
[44] P. U. Renberg, D. F. Measday, M. Pepin, P. Schwaller, B. Favier, and C. Richard-Serre, Nucl. Phys. **A183**, 81 (1979).
[45] R. E. Chrien, T. J. Krieger, R. J. Sutter, M. May, H. Palevsky, R. L. Stearns, T. Kozlowski, and T. Bauer, Phys. Rev. C **21**, 1014 (1980).
[46] Y. Alexander, J. W. Van Orden, E. F. Redish, and S. J. Wallace, Phys. Rev. Lett. **44**, 1579 (1980).